Critical behavior at nematic–smectic-A_1 phase transitions. I. High-resolution x-ray-scattering and calorimetric study of the liquid-crystal octyloxyphenylnitrobenzoyloxy benzoate

G. Nounesis*
Center for Materials Science and Engineering and Department of Chemistry, Massachusetts Institute of Technology, Cambridge, Massachusetts 02139

K. I. Blum and M. J. Young
Center for Materials Science and Engineering and Department of Physics, Massachusetts Institute of Technology, Cambridge, Massachusetts 02139

C. W. Garland
Center for Materials Science and Engineering and Department of Chemistry, Massachusetts Institute of Technology, Cambridge, Massachusetts 02139

R. J. Birgeneau
Center for Materials Science and Engineering and Department of Physics, Massachusetts Institute of Technology, Cambridge, Massachusetts 02139
(Received 18 June 1992)

High-resolution x-ray scattering and ac-calorimetric measurements have been carried out near the nematic–smectic-A_1 phase transition of the pure liquid-crystal compound octyloxyphenylnitrobenzoyloxy benzoate (DB_8ONO_2). Several forms of the structure factor $S(\mathbf{q})$ for fitting the x-ray line shape have been tested. The critical temperature dependences of the resulting longitudinal and transverse correlation lengths $\xi_\parallel$ and $\xi_\perp$ and the smectic susceptibility σ are insensitive to the detailed form of reasonable choices for $S(\mathbf{q})$. The behaviors of $\xi_\parallel$, $\xi_\perp$, and σ are analyzed here in terms of pure power laws; the effective critical exponents for the reduced temperature range 2×10^{-5}–1.2×10^{-2} are $\nu_\parallel=0.69\pm0.03$, $\nu_\perp=0.59\pm0.03$, and $\gamma=1.28\pm0.05$. Although $\nu_\parallel$ and γ are quite close to three-dimensional (3D) XY values, the system is anisotropic with $\nu_\parallel-\nu_\perp=0.10\pm0.03$. The heat-capacity data are analyzed using a nonasymptotic power-law expression with first- and second-order corrections-to-scaling terms. This analysis yields a critical exponent α which agrees with 3D XY theory: $\alpha=-0.007\pm0.003$. Thus, anisotropic hyperscaling ($\alpha+\nu_\parallel+2\nu_\perp=2$) appears to be violated if effective exponents based on pure power-law fits to x-ray data are used. However, hyperscaling can be recovered by a preasymptotic XY analysis of the x-ray data, as shown in paper II [Phys. Rev. E **47**, 1918 (1993)].

PACS number(s): 64.70.Md, 61.30.−v, 64.60.Fr, 65.20.+w

I. INTRODUCTION

The nature of the nematic (N)–smectic-A (Sm-A) phase transition in thermotropic liquid-crystalline materials has been a long-standing puzzle in the field of critical phenomena. Most theoretical studies predict that the transition should be three-dimensional (3D) XY like [1–3]. However, the experimental results to date have not established a clear case of 3D XY universality, and the possibility of a broad crossover toward an anisotropic fixed point [4] remains. A wide variety of experimental systems have been studied—both nonpolar materials exhibiting the N–Sm-A_m monomeric transition and polar materials exhibiting the nematic-partial bilayer smectic-A_d (N–Sm-A_d) transition [5–8]. None of these liquid-crystal systems show a set of critical exponents in full agreement with the 3D XY predictions. Moreover, the correlation-length critical exponents $\nu_\parallel$ and $\nu_\perp$ (where $\nu_\parallel$ and $\nu_\perp$ are the exponents describing the divergence of the correlation lengths parallel and perpendicular to the nematic director) have always been found to be anisotropic with $\nu_\parallel-\nu_\perp\simeq0.13$. The presence of two differential critical exponents describing the correlation length singularity is, of course, a serious violation of the scaling laws. The broad range of critical exponents found experimentally has been attributed in part to the proximity of the systems that have been studied so far to a tricritical point. Liquid-crystal systems with narrow nematic ranges have been studied where first-order to tricritical to second-order crossover has been well documented [6,7,9–11]. However, even in the tricritical region one finds $\nu_\parallel-\nu_\perp\simeq0.1$ [7].

Recently, ac-calorimetric studies of the critical heat-capacity behavior have been reported for several polar liquid-crystal compounds ("frustrated smectics") that exhibit the nematic-monolayer smectic-A_1 (N–Sm-A_1) transition [11–13]. These compounds are all characterized by wide nematic ranges (≥45 K). The heat capacity C_p for all these systems was found to have an ideal 3D XY behavior with a critical exponent $\alpha=-0.007\pm0.009$. Furthermore, first- and second-order corrections-to-scaling terms have been found to be important for the

description of the C_p data [12].

In the present paper, we report high-resolution x-ray-scattering and ac-calorimetric measurements near the N–Sm-A_1 phase transition of the compound octyloxyphenylnitrobenzoyloxy benzoate (DB_8ONO_2):

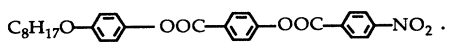

We present a detailed line-shape analysis for the x-ray-scattering data and investigate the effects of different forms for the structure factor $\mathbf{S}(\mathbf{q})$ on the resulting values of the correlation lengths $\xi_\parallel$ and $\xi_\perp$ and the smectic susceptibility σ. The dependences of $\xi_\parallel$, $\xi_\perp$, and σ on the reduced temperature $\tau=(T-T_c)/T_c$ are analyzed using pure power laws and effective critical exponents, as has been conventionally done for other N–Sm-A systems [7,8]. The C_p measurements are analyzed with a nonasymptotic form that includes first- and second-order corrections-to-scaling terms, as done previously [11,12].

Our inspiration for studying the compound DB_8ONO_2 originated from a C_p study of binary mixtures of $DB_8ONO_2+DB_{10}ONO_2$ [11]. In this system, a critical-to-tricritical crossover was observed. A mixture with $X=31.5$, where X is the mole percent $DB_{10}ONO_2$, showed ideal 3D XY heat-capacity behavior, while a mixture with $X=51.33$ exhibited tricritical behavior ($\alpha=0.50\pm0.04$). As the pure compound DB_8ONO_2 is substantially further away from this tricritical point than the $X=31.5$ mixture, it was deemed a very suitable candidate for observing ideal 3D XY behavior. DB_8ONO_2 exhibits the phase sequence [14]

$$I \xrightarrow[500\ \mathrm{K}]{} N \xrightarrow[404.25\ \mathrm{K}]{} \text{Sm-}A_1 \xrightarrow[382.1\ \mathrm{K}]{} \text{Sm-}\tilde{C} \xrightarrow[364.7\ \mathrm{K}]{} \text{cryst.},$$

and thus has a nematic range of 96 K.

This paper is organized as follows: The experimental results from the x-ray scattering and their analysis are presented in Sec. II; the C_p results and analysis are given in Sec. III; and finally our conclusions are discussed in Sec. IV. A detailed *preasymptotic* 3D XY analysis of the x-ray data and a discussion of universality issues in the context of an overall analysis of both C_p and $\xi_\parallel\xi_\perp^2$ is given in the following paper (paper II) for DB_8ONO_2 together with four other N-Sm-A_1 systems [15].

II. X-RAY SCATTERING

The x-ray scattering experiment was carried out in an experimental setup that used the Cu $K\alpha$ x rays from a Rigaku Ru-300 rotating-anode source operating at 12 kW. A standard four-circle spectrometer was used in the nondispersive configuration with Si(111) single crystals as monochromator and analyzer. The longitudinal resolution was 1.3×10^{-4} Å^{-1} half width at half maximum (HWHM). The transverse in-plane resolution was nearly perfect, while the transverse out-of-plane resolution, dependent only on the slit settings, was best described by a Gaussian with 0.04 Å^{-1} HWHM. A liquid-crystal sample with a mass of 160 mg was sealed in a flat rectangular beryllium cell $12\times12\times1.5$ mm^3. The temperature was controlled by a two-stage beryllium oven which gave a temperature stability of better than ±2 mK. This determined the experimental temperature resolution. The vertical temperature gradient across the 12-mm height of the sample was 1 mK, and a total sample area of 1 mm$\times$3.5 mm was illuminated by x rays. The liquid-crystal molecules were aligned in the nematic phase by a 6.5-kG electromagnet. Longitudinal (parallel to the director) and transverse scans were carried out at a series of constant temperatures in the nematic phase.

The DB_8ONO_2 sample was synthesized and purified at the Technical University of Berlin and was from the same batch as the material used in the study of $DB_8ONO_2+DB_{10}ONO_2$ mixtures [11]. The transition temperature T_c was determined by the appearance of mosaic structure in the transverse scan, as shown in Fig. 1(a). The mosaicity of the DB_8ONO_2 sample was found to be 0.24° HWHM. Initially we found $T_c=404.254$ K, but the T_c value drifted slowly with time. Because of this thermal drift, T_c was measured twice daily and time-dependent T_c values were used to calculate the reduced temperature value τ for each run. For the first seven days we recorded drift rates of $dT_c/dt\simeq-45$ mK/day. These rates then became slower, and for the rest of the experiment were -20 mK/day. Data obtained over an extensive period of time are internally consistent as a function of $T-T_c$. Thus the effect of slow changes in the sample purity at high temperatures causes merely a shift in T_c but not a change in the critical behavior.

In the nematic phase near the N–Sm-A_1 phase transition, the diffuse x-ray peak associated with the Sm-A_1 fluctuations was centered at $2\mathbf{q}_0=(0,0,0.2097)$, which corresponds to a layer spacing $d=(2\pi/2q_0)=29.96$ Å. No temperature dependence was found for $2q_0$ in the nematic phase or in the Sm-A_1 phase just below the transition. Displayed in Fig. 1 are longitudinal scans $(0,0,q_\parallel)$ and transverse scans $(q_\perp,0,0.2097)$ at four reduced temperatures. The overall scattering profiles are very similar to those of other N–Sm-A phase transitions studied previously [7,8].

One interesting feature of the DB_8ONO_2 data is the presence of a second diffuse x-ray peak centered at $\mathbf{q}_0'=(0,0,0.1443)$, as can be seen in Fig. 2. This peak, associated with short-range partial bilayer (Sm-A_d) order, corresponds to a layer spacing $d'=(2\pi/q_0')=43.54$ Å. Such Sm-A_d-like fluctuations are expected [16] in the nematic phase of a frustrated smectic system even if it does not exhibit a stable long-range ordered Sm-A_d phase at any temperature. The q_0' peak position, intensity, and

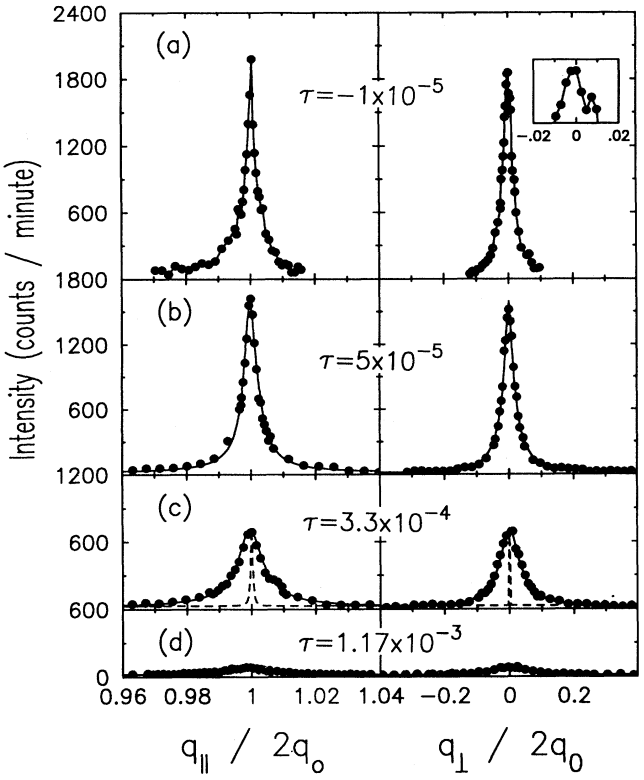

FIG. 1. Longitudinal and transverse x-ray scans in DB_8ONO_2 at four reduced temperatures $\tau=(T-T_c)/T_c$. The solid lines in (*b*)–(*d*) are least squares-fits with Eq. (1) convoluted with the instrumental resolution [shown as dashed curves in part (*c*)]. The lines in part (*a*) are merely guides for the eye; the inset shows the mosaic in the Sm-A_1 phase.

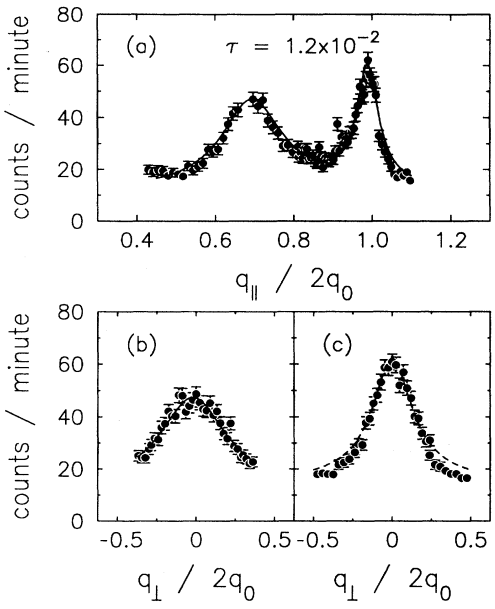

FIG. 2. Longitudinal (a) and transverse (b) and (c) x-ray scans in DB_8ONO_2 at $\tau=1.2\times10^{-2}$, where the Sm-A_1 diffuse peak is centered at $2\mathbf{q}_0=(0,0,0.2097)$ and a second diffuse peak associated with Sm-A_d can be seen at $\mathbf{q}_0'=(0,0,0.1443)$. Scan (b) is through the q_0' peak, and scan (c) is through the $2q_0$ peak. The solid lines represent a fit to the $2\mathbf{q}_0$ peak with Eq. (1) and the q_0' feature with a Lorentzian form. The dashed profile in part (c) is the best fit to the transverse scan through the $2q_0$ peak with a Lorentzian form, i.e., Eq. (1) with c held equal to zero.

width show no temperature dependence. All aspects of this weak, diffuse peak are absolutely stable not only in the nematic phase but also in the Sm-A_1 phase down to 5 K below T_c. A similar diffuse peak has been detected in an x-ray study of the binary mixture $DB_8ONO_2+DB_{10}ONO_2$ at a q_0' value different from the q_0'' value of the quasi-Bragg spot associated with the long-range Sm-A_d phase observed in this mixture [17]. Although the Sm-A_d-like q_0' peak in DB_8ONO_2 becomes comparable in intensity to the Sm-A_1 peak only for $\tau>10^{-2}$, its presence was taken into account in the line-shape analysis of all our data. Both longitudinal and transverse scans through the q_0' peak could be well described by a Lorentzian, as shown in Figs. 2(a) and 2(b). This peak with a temperature-independent longitudinal HWHM of 1.59×10^{-2} Å^{-1} and transverse HWHM of 5.58×10^{-2} Å^{-1} was treated as part of the background.

Sm-A_1 fluctuations in the nematic phase are described by the following structure factor expression:

$$S(\mathbf{q})=\sigma/[1+\xi_{\parallel}^2(q_{\parallel}-2q_0)^2+\xi_{\perp}^2q_{\perp}^2+c\xi_{\perp}^4q_{\perp}^4]\ , \qquad (1)$$

convoluted with the resolution function. No corrections for mosaicity were needed. Equation (1) contains the quartic term $c\xi_{\perp}^4q_{\perp}^4$, as is conventional in analysis of N–Sm-A data [8,18]. The need for a quartic term, which most probably has its origin in splay-mode director fluctuations, is dictated by the non-Lorentzian wings of transverse scans at large τ, as first shown by Als-Nielsen *et al.* [18]. Figure 2(c) displays the results of fitting a transverse scan at $\tau=1.2\times10^{-2}$ with Eq. (1) allowing $c\neq0$ and with a Lorentzian (i.e., $c=0$). It is obvious that a fourth-order term is needed to fit these data adequately. The coefficient c is a freely adjustable parameter in the fits and its temperature dependence is shown in Fig. 3.

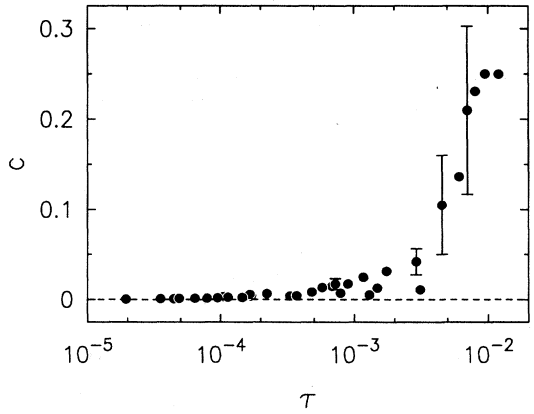

FIG. 3. Fourth-order coefficient c in Eq. (1) obtained from least-squares fits to the x-ray profile. The error bars for $\tau<3\times10^{-4}$ are smaller than the plotted points.

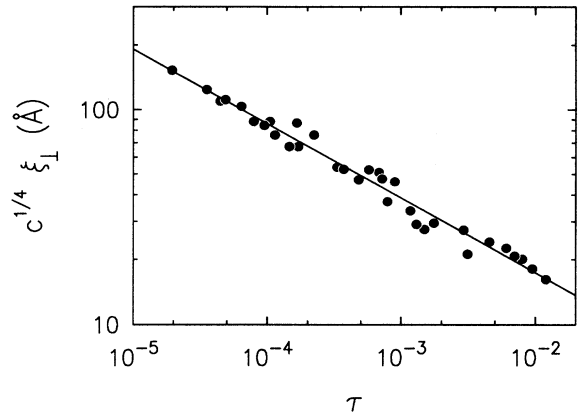

FIG. 4. Dependence of $\xi_s \equiv c^{1/4}\xi_\perp$ on reduced temperature. The line represents the empirical form $\xi_{s0}\tau^{-\nu_s}$ with $\xi_{s0}=5.14$ Å and $\nu_s=0.35$.

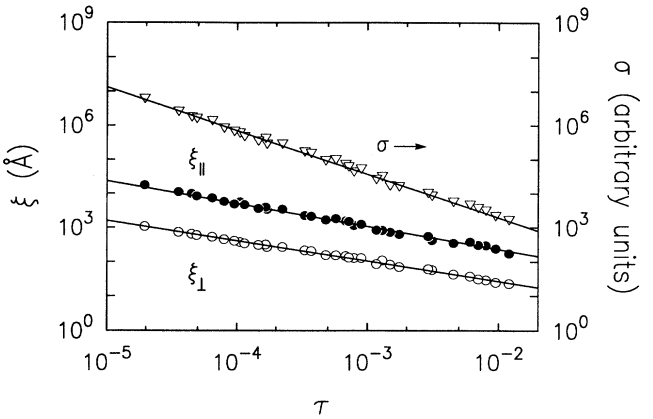

FIG. 5. Smectic-A_1 susceptibility σ and the longitudinal and transverse correlation lengths $\xi_\parallel$ and $\xi_\perp$ near the N-Sm-A_1 transition in DB_8ONO_2. The lines are least-squares fits with pure power laws, and the fitting parameters are given in the first line of Table I. The σ values have been shifted up by a factor of 4 to improve the clarity.

One sees that c is very small near T_c and never becomes larger than 0.25 far away from T_c, in agreement with the results of fits to x-ray data for other N–Sm-A systems [7,8]. This temperature dependence of c reflects a crossover in the transverse line shape, which changes from a Lorentzian near T_c to a Lorentzian squared at large τ.

It has recently been argued [19] that a more correct form for Eq. (1) should have the quartic term $\xi_s^4 q_\perp^4$ instead of $c\xi_\perp^4 q_\perp^4$, where ξ_s is a splay correlation length; it is further argued that ξ_s should be constrained to a power-law critical behavior $\xi_{s0}\tau^{-\nu_s}$ characterized by a critical exponent ν_s. The empirical ν_s and ξ_{s0} values reported for octyloxyphenylcyanobenzoyloxy benzoate (8OPCBOB) are $\nu_s \simeq 0.41$ and $\xi_{s0}=2.33$ Å [19]. Figure 4 displays our quantity $c^{1/4}\xi_\perp$ as a function of τ for DB_8ONO_2. These points can be fitted nicely by a pure power law with an exponent equal to 0.35 ± 0.05. Thus, Fig. 4 demonstrates that the treatments of the transverse line shape with Eq. (1) or with a form that includes a $\xi_s^4 q_\perp^4$ splay term are equivalent as, of course, they must be since they are algebraically identical except for the power-law constraint imposed in Ref. 19. It has also been argued [19] that the critical behavior of ξ_s affects the criticality of the correlation length $\xi_\perp$. As shown below, the statistics of our data analysis do not show such a trend. The uncertainty in the determination of $\xi_\perp$ from fitting the data with different $S(\mathbf{q})$ has *no significant effect* on the values of the effective critical exponents, at least within the experimental standard deviations.

The values of $\xi_\parallel$, $\xi_\perp$, and the smectic susceptibility σ obtained from fits to the x-ray profiles with Eq. (1) are shown in Fig. 5. These quantities have been fitted over the range $2\times10^{-5}<\tau<1.2\times10^{-2}$ with pure power-law expressions having the forms

$$\xi_\parallel=\xi_{\parallel 0}\tau^{-\nu_\parallel},\quad \xi_\perp=\xi_{\perp 0}\tau^{-\nu_\perp},\quad \sigma=\sigma_0\tau^{-\gamma}\ . \tag{2}$$

The 3D XY values for the critical exponents are $\nu_\parallel=\nu_\perp=0.669\pm0.001$ and $\gamma=1.316\pm0.002$ [20]. As can be seen from Table I, our results for $\nu_\parallel$ and γ seem to agree with the 3D XY values within the experimental uncertainties but the value of $\nu_\perp$ does not. The observed anisotropy in the correlation length exponents is reflected in the temperature dependence of the ratio $\xi_\parallel/\xi_\perp$, which is shown in Fig. 6. It should be noted that the form of $S(\mathbf{q})$ given in Eq. (1) can be trivially rewritten so that σ, $\xi_\parallel$, and $(\xi_\perp/\xi_\parallel)$ are the three adjustable parameters in least-squares fits to each pair of scattering profiles. The ratios in Fig. 6 were determined in this way and are more reliable than values obtained by simply dividing $\xi_\parallel$ by $\xi_\perp$ using the values in Fig. 5.

To demonstrate the effects of the quartic term on the

TABLE I. Least-squares values of the amplitudes and effective critical exponents for $\xi_\parallel$, $\xi_\perp$, and σ using the pure power-law forms given in Eqs. (2) and three different forms for the structure factor $S(\mathbf{q})$. The units of $\xi_{\parallel 0}$ and $\xi_{\perp 0}$ are Å^{-1}; those of σ are arbitrary. The uncertainties are 95% confidence limits.

$S(\mathbf{q})$	$\xi_{\parallel 0}$	$\nu_\parallel$	$\xi_{\perp 0}$	$\nu_\perp$	σ_0	γ
Eq. (1), $c\neq0$	8.74	0.69	1.75	0.59	1.33	1.28
	±0.44	±0.03	±0.09	±0.03	±0.05	±0.05
Eq. (1), $c=0$	9.01	0.71	2.55	0.59	1.77	1.27
	±0.50	±0.03	±0.14	±0.03	±0.10	±0.05
Eq. (3)	8.39	0.69	1.00	0.60	1.39	1.27
	±0.46	±0.04	±0.05	±0.04	±0.08	±0.06

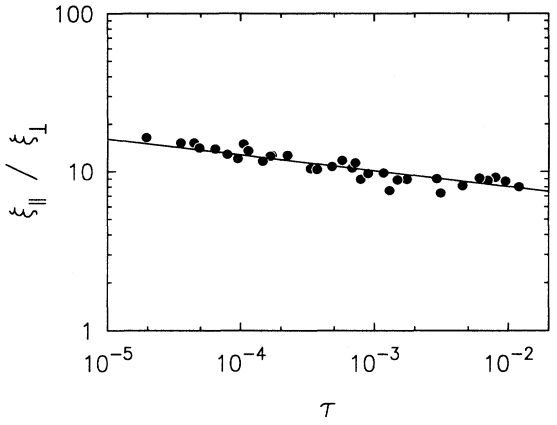

FIG. 6. Ratio $\xi_\parallel/\xi_\perp$ of correlation lengths. The best-fit line has a slope $\Delta\nu=\nu_\parallel-\nu_\perp=0.10$.

values of the critical exponents, we have also fit our data by (a) setting c equal to zero in Eq. (1) for all temperatures and (b) using the empirical Lorentzian term with a power-law correction given by [7,18]

$$S(\mathbf{q})=\frac{\sigma}{\xi_\parallel^2(q_\parallel-2q_0)^2+(1+\xi_\perp^2 q_\perp^2)^{1-\eta_\perp/2}}\ , \tag{3}$$

where $-2<\eta_\perp<0$ is an empirical τ-dependent exponent that is freely adjustable in the fits. This form of $S(\mathbf{q})$, like Eq. (1), changes from Lorentzian near T_c (where $\eta_\perp\simeq 0$) to Lorentzian squared far from T_c (where $\eta_\perp=-2$). The profiles were almost as well fit with Eq. (3) as Eq. (1) with $c\neq 0$, but the Lorentzian form provided poorer fits. Figure 7 shows the values for $\xi_\perp$ obtained using these three different structure factor forms. Comparable effects are also obtained for $\xi_\parallel$ and σ, and Table I lists the amplitudes and effective exponents obtained from power-law fits. It is evident from Fig. 7 and Table I that the fourth-order term in Eq. (1) has no significant effect on the values of the experimental critical exponents although the amplitudes are variable depending on the assumed form for $S(\mathbf{q})$. Equivalent results have been obtained previously [7].

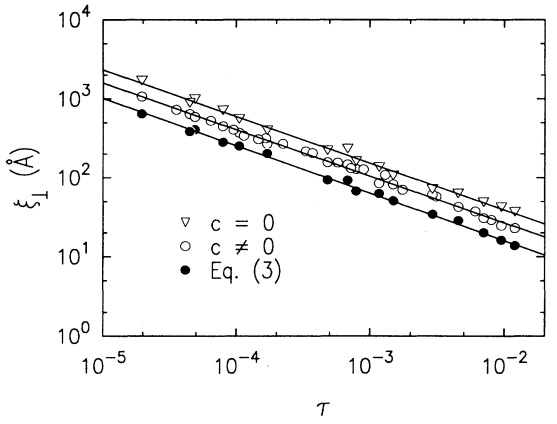

FIG. 7. Influence of the form of the structure factor $S(\mathbf{q})$ on the transverse correlation length $\xi_\perp$ in DB_8ONO_2. The points denoted by open circles (○) and triangles (▽) were obtained by fitting the x-ray profile with Eq. (1) with $c\neq 0$ and $c=0$, respectively. The solid points (●) came from fits to the profile with Eq. (3) with $\eta_\perp$ taken to be a freely adjustable parameter at each temperature. A subset of the DB_8ONO_2 data shown in Fig. 5 were used here. The least-squares parameters for the power-law fits shown by the straight lines are given in Table I.

III. CALORIMETRY

The C_p measurements on DB_8ONO_2 were carried out in a fully automated ac-calorimeter which has been described in detail elsewhere [11,21]. The mass m of the DB_8ONO_2 sample was 0.060 g, and this sample was sealed inside a silver cell. The C_p values were obtained from the following expression:

$$C_p=[C_p(\text{obs})-C_p(\text{empty})]/m\ , \tag{4}$$

where C_p(obs) is the observed heat capacity of the filled cell and C_p(empty) is the heat capacity of the empty cell. C_p(empty) exhibits only a very small linear temperature dependence over the range of interest. The recorded drifts in T_c for the C_p sample were similar to those obtained from the x-ray equipment: $dT_c/dt=-20$ mK/day. The C_p data are displayed in Fig. 8. For the analysis we used the following renormalization-group expression which contains first- and second-order corrections-to-scaling terms [12]

$$C_p^{\pm}=A^{\pm}|\tau|^{-\alpha}(1+D_1^{\pm}|\tau|^{\Delta_1}+D_2^{\pm}|\tau|^{\Delta_2})+B\ . \tag{5}$$

Here the superscripts $\pm$ indicate above and below the transition temperature. $A^{\pm}$ is the critical amplitude; the constant term B contains a regular background contribution B_{reg} and a critical contribution B_c such that $B=B_{\text{reg}}+B_c$. $D_1^{\pm}$ and $D_2^{\pm}$ are the coefficients of the

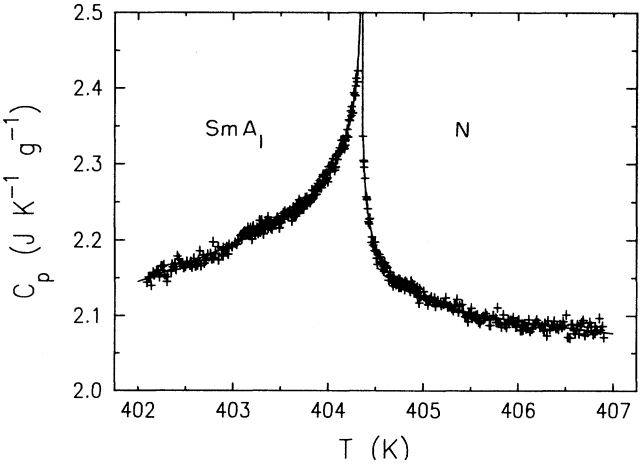

FIG. 8. Heat capacity near the N-Sm-A_1 transition in DB_8ONO_2. The reduced temperature range of the fit with Eq. (5) is $-6\times10^{-3}<\tau<+6\times10^{-3}$, and the line represents fit 4 in Table II. The standard deviation in measured C_p values is ±0.005 J K^{-1} g^{-1}.

TABLE II. Values of the adjustable parameters obtained from least-squares fits of the C_p data with Eq. (5). The units of A^+ and B are $\mathrm{J\,K^{-1}\,g^{-1}}$. Brackets denote that the variable was held fixed at the given value. The ranges of these fits are $|\tau|<10^{-3}$ (range A), $|\tau|<3\times10^{-3}$ (range B), and $|\tau|<6\times10^{-3}$ (range C). Uncertainties are 95% confidence limits based on F tests for each data set (433 points for range C).

Fit	Range	T_c (K)	α	A^+	A^-/A^+	B	D_1^+	D_1^-/D_1^+	D_2^+	D_2^-/D_2^+	χ_ν^2
1	A	404.354	−0.008	−10.03	0.980	11.60	−0.19	0.25	[0]	[1]	1.33
		±0.001	±0.003	±0.20	±0.003	±0.23	±0.07	±0.09			
2	B	404.354	−0.006	−11.08	0.983	12.68	−0.17	0.11	[0]	[1]	1.28
		±0.001	±0.003	±0.17	±0.003	±0.19	±0.06	±0.04			
3	C	404.357	−0.005	−11.71	0.983	13.40	−0.09	−0.54	[0]	[1]	1.35
		±0.001	±0.003	±0.15	±0.003	±0.17	±0.05	±0.14			
4	C	404.351	[−0.007]	−12.88	0.986	14.31	−0.30	0.72	1.27	1.33	0.95
		±0.001		±0.17	±0.003	±0.19	±0.07	±0.18	±0.32	±0.33	

first- and second-order corrections-to-scaling terms, respectively; while Δ_1 and Δ_2 are the correction exponents. We have used $\Delta_1=0.5$ and $\Delta_2=2\Delta_1=1$ [12]. A few data points very close to T_c had to be excluded from the fits (rounded data points due to instrumental limitations). Fits were carried out for a range $\tau_{\min}<\tau<\tau_{\max}$, where $\tau_{\min}=-9\times10^{-5}$ and $+4\times10^{-5}$ for all fits and three different values were taken for $\tau_{\max}$ so that the stability of the fit parameter values could be tested with range shrinking. The three different maximum ranges used were $|\tau_{\max}|=10^{-3}$ (range A), $|\tau_{\max}|=3\times10^{-3}$ (range B), and $|\tau_{\max}|=6\times10^{-3}$ (range C).

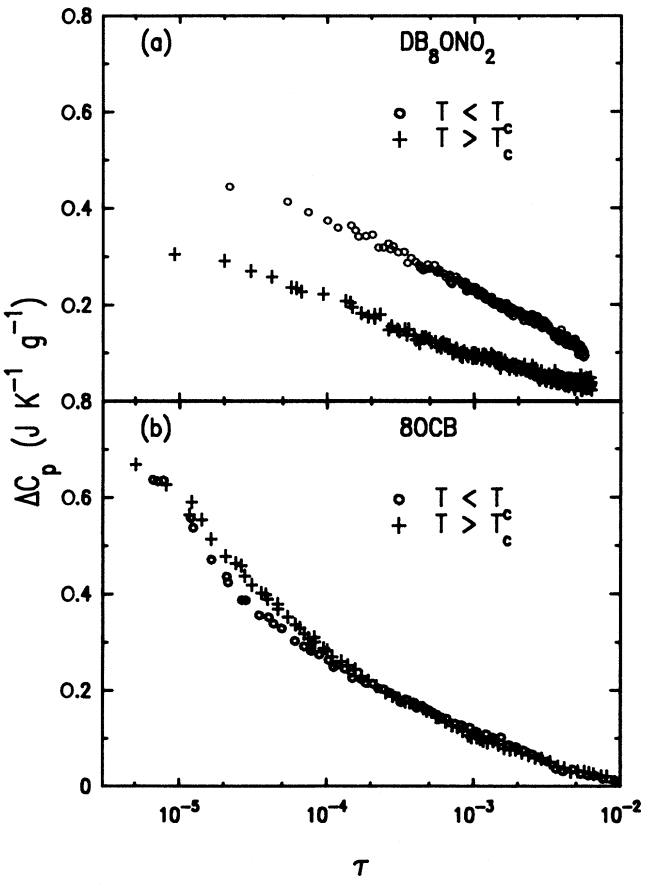

FIG. 9. Semilogarithmic plot of ΔC_p vs τ for (a) DB_8ONO_2 and (b) octyloxycyanobiphenyl (8OCB). The 8OCB data are taken from Ref. [23] and are characterized by $\alpha\simeq+0.2$. Note the curvature of the 8OCB data and the difference between $T>T_c$ data and $T<T_c$ data for DB_8ONO_2.

Table II lists the values of the critical exponent α, the amplitude A^+, the ratio A^-/A^+, and the other adjustable parameters for four fits with Eq. (5). For fits 1–3, α is free and the second-order correction terms are set to zero, i.e., $D_2^\pm=0$. To show the importance of the $D_2^\pm$ terms in fitting C_p data outside range B, fit parameters are also shown for fit 4, where α is fixed at the 3D XY value $\alpha_{XY}=-0.007$ and $D_2^\pm$ coefficients are freely adjustable parameters. This fit, which yields a D_1^-/D_1^+ ratio close to the theoretical value of $+1$, is displayed in Fig. 8. It is evident from the χ_ν^2 and D_1^-/D_1^+ values given in Table II that the $D_2^\pm\tau$ terms are essential for representing the C_p variation over range C, which is consistent with the behavior of C_p(N-Sm-A_1) in other systems [11,12]. Note also that the C_p data conform well with the normal 3D XY model, for which the theoretical value of A^-/A^+ is 0.9714±0.0126 [22], rather than the inverted XY model. The DB_8ONO_2 amplitude ratio agrees well with those observed in other N-Sm-A_1 systems.

It should be emphasized at this point that the 3D XY character of the C_p data for DB_8ONO_2, as well as that for other N-Sm-A_1 compounds [12], is not simply the effect of using many parameters in the least-squares fitting. Figure 9(a) displays $\Delta C_p=C_p-B_{\mathrm{reg}}$, where B_{reg} is the temperature-independent regular background contribution. It is obvious from this semilogarithmic plot that the ΔC_p variation for DB_8ONO_2 is quite close to a logarithmic singularity ($\alpha=0$) and certainly does not agree with a $\alpha>0$ divergence like that for 8OCB [23], which is shown in Fig. 9(b). ΔC_p for DB_8ONO_2 behaves much like that for liquid helium [24]. Indeed, the deviations observed at large τ are qualitatively the same as those in He and are accounted for by the corrections-to-scaling terms.

IV. CONCLUSIONS

The x-ray-scattering measurements on DB_8ONO_2 reveal that although the effective critical exponents $\nu_\parallel$ and

γ conform well with 3D XY universality, $\nu_\perp$ does not. Once again in this system, as in previously studied ones, the correlation length exponents are anisotropic with $\nu_\parallel - \nu_\perp = 0.10 \pm 0.03$. Our line-shape analysis provides no evidence that this anisotropy is the result of the way the transverse line shapes were analyzed, in disagreement with the suggestion of Ref. [19]. It should be stressed that the detailed form of reasonable choices for the structure factor $S(\mathbf{q})$ has no serious influence on the values of the effective critical exponents that are obtained from pure power analysis. Comments in Ref. [19] concerning differences between correlation exponents in the so-called "liquid-crystal" and "superconducting" gauges are incorrect. Specifically, in a series of careful x-ray- and light-scattering experiments [5,25] it has been shown that the x-ray lengths and the "elastic constant" lengths are quantitatively identical.

The C_p results are in excellent agreement with the 3D XY universality class predictions. An additional test of universality is the amplitude ratio $R_{B_c}^+$. As pointed out by Bagnuls and Bervillier [26], $R_{B_c}^+ \equiv A^+ |D_1^+|^{\alpha/\Delta_1} B_c^{-1}$ is a universal quantity with a 3D XY value of $= -1.057 \pm 0.022$. If $B_{\rm reg} = 2.05$ is chosen to be the C_p value very far away from T_c, we find $B_c = 12.26 \pm 0.19$. This yields $R_{B_c}^+ = -1.068 \pm 0.027$, in excellent agreement with theory. The amplitude ratio A^-/A^+, as in previously studied systems, is in compliance with the value for the orthodox 3D XY model and not with the theoretically predicted inverted value. It should be noted, however, that a Monte Carlo simulation [27] of the de Gennes model shows noninverted C_p critical behavior. The importance of the first- and second-order corrections-to-scaling terms is once again underlined by the C_p results.

A further test of universality is hyperscaling. From two-scale-universality free energy considerations, one obtains

$$\nu_\parallel + 2\nu_\perp + \alpha = 2 \tag{6}$$

as the anisotropic hyperscaling relation [3]. The x-ray and C_p results quoted above for DB_8ONO_2 yield $\nu_\parallel + 2\nu_\perp + \alpha = 1.86 \pm 0.07$ when Eq. (1) is used as the structure factor $S(\mathbf{q})$ and 1.88 ± 0.09 when Eq. (3) is used for $S(\mathbf{q})$. These uncertainty limits are 95% confidence limits based on a propagation-of-error treatment using the uncertainties listed in Table I and $\Delta(\alpha) = \pm 0.003$. Thus it would appear that hyperscaling is violated in this system, as in the case of the compound 8OPCBOB studied in Ref. [19]. These apparent violations in polar N–Sm-A_1 systems arise from the use of effective exponents $\nu_\parallel$ and $\nu_\perp$ obtained from the use of pure power laws to describe the critical behavior of $\xi_\parallel$ and $\xi_\perp$. A preasymptotic analysis of the x-ray data using corrections-to-scaling terms, presented in paper II, shows that hyperscaling is indeed obeyed. Paper II also discusses the possible influence of the anisotropic fixed point first proposed by Nelson and Toner [4].

ACKNOWLEDGMENTS

We wish to thank G. Heppke and R. Shashidhar for providing a high-quality DB_8ONO_2 sample. This work was supported by National Science Foundation Grants Nos. DMR90-07611 and DMR90-22933.

*Present address: Francis Bitter National Magnet Laboratory, MIT, Cambridge, MA 02139.

[1] P. G. de Gennes, Solid State Commun. **10**, 753 (1972); Mol. Cryst. Liq. Cryst. **21**, 49 (1973); *The Physics of Liquid Crystals* (Clarendon, Oxford, 1974).

[2] B. I. Halperin, T. C. Lubensky, and S. K. Ma, Phys. Rev. Lett. **32**, 292 (1974); C. Dasgupta and B. I. Halperin, *ibid.* **47**, 1556 (1981).

[3] T. C. Lubensky, J. Chim. Phys. **80**, 31 (1983), and references cited therein.

[4] D. R. Nelson and J. Toner, Phys. Rev. B **24**, 363 (1981); B. R. Patton and B. S. Andereck, Phys. Rev. Lett. **69**, 1556 (1992).

[5] D. L. Johnson, J. Chim. Phys. **80**, 45 (1983), and references cited therein; C. W. Garland, M. Meichle, B. M. Ocko, A. R. Kortan, C. R. Safinya, J. J. Yu, J. D. Litster, and R. J. Birgeneau, Phys. Rev. A **27**, 3234 (1983), and references cited therein.

[6] J. Thoen, H. Marynissen, and W. VanDael, Phys. Rev. Lett. **52**, 204 (1984).

[7] B. M. Ocko, R. J. Birgeneau, and J. D. Litster, Z. Phys. B **62**, 487 (1986).

[8] K. W. Evans-Lutterodt, J. W. Chung, B. M. Ocko, R. J. Birgeneau, C. Chiang, C. W. Garland, E. Chin, J. Goodby, and N. H. Tinh, Phys. Rev. A **36**, 1387 (1987).

[9] K. J. Stine and C. W. Garland, Phys. Rev. A **39**, 3148 (1989).

[10] D. Brisbin, R. De Hoff, T. F. Lockhart, and D. L. Johnson, Phys. Rev. Lett. **43**, 1171 (1979).

[11] G. Nounesis, C. W. Garland, and R. Shashidhar, Phys. Rev. A **43**, 1849 (1991).

[12] C. W. Garland, G. Nounesis, and K. J. Stine, Phys. Rev. A **39**, 4919 (1989); C. W. Garland, G. Nounesis, K. J. Stine, and G. Heppke, J. Phys. (Paris) **50**, 2291 (1989).

[13] L. Wu, C. W. Garland, and S. Pfeiffer, Phys. Rev. A **46**, 973 (1992); **46**, 6761(E) (1992).

[14] V. N. Raja, R. Shashidhar, B. R. Ratna, G. Heppke, and Ch. Bahr, Phys. Rev. A **37**, 303 (1988).

[15] C. W. Garland, G. Nounesis, M. J. Young, and R. J. Birgeneau, following paper, Phys. Rev. E **47**, 1918 (1993); this is denoted as paper II.

[16] P. Barois, J. Prost, and T. C. Lubensky, J. Phys. (Paris) **46**, 391 (1985).

[17] G. Nounesis, K. Blum, C. W. Garland, R. J. Birgeneau, S. Pfeifer, and R. Shashidhar (unpublished).

[18] J. Als Nielsen, R. J. Birgeneau, M. Kaplan, J. D. Litster, and C. R. Safinya, Phys. Rev. Lett. **39**, 352 (1977); B. M. Ocko, Ph.D. thesis, Massachusetts Institute of Technology, 1984.

[19] W. G. Bouwman and W. H. de Jeu, Phys. Rev. Lett. **68**, 800 (1992).

[20] C. Bagnuls and C. Bervillier, Phys. Rev. B **32**, 7209 (1985).

[21] C. W. Garland, Thermochim. Acta **88**, 127 (1985).

[22] C. Bervillier, Phys. Rev. B **34**, 8141 (1986).

[23] C. W. Garland, G. B. Kasting, and K. J. Lushington, Phys. Rev. Lett. **43**, 1420 (2979), see Fig. 3(a).
[24] G. Ahlers, in *The Physics of Liquid and Solid Helium,* edited by K. H. Bennemann and J. B. Ketterson (Wiley, New York, 1976), Pt. 1, Chap. 2, see Fig. 2.9; see also G. Ahlers, Phys. Rev. A **3**, 696 (1971).
[25] S. Sprunt, L. Solomon, and J. D. Litster, Phys. Rev. Lett. **53**, 1923 (1984).
[26] C. Bagnuls and C. Bervillier, Phys. Lett. **112A**, 9 (1985).
[27] C. Dasgupta, J. Phys. (France) **48**, 957 (1987).